

Nonlinear model to predict the torsional response of U-shaped thin-walled RC members

Shenggang Chen¹, Yinghua Ye^{1,2}, Quanguan Guo^{*1}, Shaohong Cheng³
and Bo Diao^{1,2}

¹Department of Civil Engineering, Beihang University, Beijing, 100191, China

²State Key Laboratory of Subtropical Building Science South China University of Technology, Guangzhou, 510641, China

³Department of Civil and Environmental Engineering, University of Windsor, Windsor, Ontario N9B 3P4, Canada

(Received August 1, 2016, Revised October 6, 2016, Accepted October 7, 2016)

Abstract. Based on Vlasov's torsional theory of open thin-walled members and the nonlinear constitutive relations of materials, a nonlinear analysis model to predict response of open thin-walled RC members subjected to pure torsion is proposed in the current study. The variation of the circulatory torsional stiffness and warping torsional stiffness over the entire loading process and the impact of warping shear deformation on the torsion-induced rotation of the member are considered in the formulation. The torque equilibrium differential equation is then solved by Runge-Kutta method. The proposed nonlinear model is then applied to predict the behavior of five U-shaped thin-walled RC members under pure torsion. Four of them were tested in an earlier experimental study by the authors and the testing data of the fifth one were reported in an existing literature. Results show that the analytical predictions based on the proposed model agree well with the experimental data of all five specimens. This clearly shows the validity of the proposed nonlinear model analyzing behavior of U-shaped thin-walled RC members under pure torsion.

Keywords: U-shaped RC members; thin-walled members; warping torsion; nonlinear stiffness; warping shear deformation

1. Introduction

The application of U-shaped thin-walled reinforced concrete members (UTWRCMs) to the construction of urban rail viaduct has become more and more popular. However, compared to closed section members, the much lower torsional stiffness of open section members is a main drawback. To reduce the risk of potential failure of open thin-walled RC members caused by low torsional stiffness, it is imperative to develop an analytical model which would allow a better understanding of the behavior of UTWRCMs in pure torsion over the entire loading process. Since the effect of warping cannot be ignored in the torsional response of an open section member, it is very challenging to analyze the behavior of open thin-walled RC members in pure torsion.

*Corresponding author, Assistant Professor, E-mail: qq_guo@buaa.edu.cn

Remarkable progress has been made since the 1950s in the linear analysis of elastic torsional response of open thin-walled members with the consideration of warping torsion. In particular, the significant contribution made by Timoshenko (1945), Vlasov (1984), as well as Kollbrunner and Basler (Kollbrunner and Basler 2013) are worth mentioning. The linear theory for analyzing torsional behavior of open thin-walled elastic members or the Vlasov's theory was developed in 1961. By computing the warping torsion and the warping moment based on the sectorial area coordinate system, the linear analysis of open thin-walled section elastic members in torsion was made simple and possible. In recent years, how to calculate the shear deformation induced by the warping torsion (Pavazza 2005, Erkmen and Mohareb 2006, Murin and Kutíš 2008, Aminbaghai, Murin *et al.* 2016) ignored in the Vlasov's theory becomes one of the research focuses in the field. Nevertheless, all of these efforts were still within the framework of linear elastic analysis. In the case of a RC member, however, once concrete cracks, tension in the member would be solely resisted by the reinforcements in the tension zone. Both material properties and structural behavior would manifest strong nonlinearity. Therefore, the existing linear elastic theory is no longer applicable to study the post-cracking torsional performance of RC members. To the knowledge of the authors, analytical and experimental studies on the post-cracking behavior of open thin-walled RC members in torsion are quite scarce.

In 1968, Zbirohowski-Koscia (1968) made the first attempt to extend Vlasov's elastic theory to analyze stress distribution of cracked open thin-walled reinforced and prestressed concrete beams in elastic range when under the combined effect of axial force bending moments and bimoments. Subsequently, Krpan and Collins (1981a, 1981b) conducted an experimental study to investigate the post-cracking behavior and inelastic warping torsion response of a 6.4m long fixed-fixed U-shaped thin-walled specimen subjected to a torque applied at the mid-span. A theoretical model was proposed to predict the torques corresponding to the stages of concrete cracking, reinforcement yielding and specimen failure. Although only one specimen was tested and the test was terminated by an unexpected anchorage failure, the experimental results and the proposed theoretical model still provided a basic and systematic comprehension for the torsional behavior of UTWRCMs. Hwang and Hsu (1983) analyzed the torsional response of simply supported U-shaped beams in an experimental study. The torsional equilibrium differential equation was solved by applying a Fourier Series approach. However, since the circulatory torsional stiffness and the warping torsional stiffness, especially their values in the post-cracking stage, were computed using a simplified approach (Collins 1973, Hwang and Hsu 1983), a sizable discrepancy between the predicted response and the experimental data was observed. Despite the fact that the Space Truss Analogy has been continuously developed since the middle of the 20th century and the variation of the circulatory torsional stiffness over the entire loading process can now be accurately obtained (Jeng and Hsu 2009, Bernardo, Andrade *et al.* 2012, Bernardo, Andrade *et al.* 2015), besides some efforts on determining the elastic warping torsional stiffness (Waldron 1986, Kollbrunner and Basler 2013), approaches to properly evaluate the warping torsional stiffness of open thin-walled RC members after concrete cracks can rarely be found in literature.

Luccioni, Reimundin *et al.* (1991) tested the response of eight I-shaped prestressed concrete beams under combined torsion, flexure and shear and proposed a simple method for predicting bearing capacity based on the skew bending theory. Subsequently, they developed an associated computer program to reproduce the behavior of prestressed concrete I-beams under combined loads (Luccioni, Reimund *et al.* 1996). The theoretical predictions were found to agree well with the experimental results (Luccioni, Reimund *et al.* 1996). However, the approach developed in (Luccioni, Reimund *et al.* 1991) and (Luccioni, Reimund *et al.* 1996) are not applicable to

UTWRCMs because of the considerable difference in the geometrical properties between the I-shaped and the U-shaped cross sections. Little progress has been made in the field of torsional response of open thin-walled RC members in the last two decades.

Four large size U-shaped thin-walled RC members have been designed and tested under pure torsion in an earlier experimental study by our research group (Chen, Diao *et al.* 2016). By analyzing the crack development, the stress and strain status, as well as the failure mode, a simple yet effective method for computing ultimate torque was proposed. In the current study, an effort is made to develop a nonlinear model to analyze the behavior of UTWRCMs in pure torsion. The nonlinear warping torsional stiffness of the member over the entire loading history is calculated based on Vlasov’s elastic theory and the nonlinear constitutive relation of concrete and steel bars. The circulatory torsional stiffness is computed by the modified variable angle truss model (Bernardo, Andrade *et al.* 2012). The torsional rotation of the member is determined by solving the torque equilibrium differential equation using Runge-Kutta method (McGuire, Gallagher *et al.* 2000). The combined effect of circulatory torsion and warping torsion, and the possible amplification of warping shear deformation on the member rotational angle are considered in the formulation of the proposed nonlinear model. The model is then applied to analyze the torsional response of the specimens tested in (Chen, Diao *et al.* 2016), of which a good agreement with the experimental data is found. This verifies the validity of the proposed nonlinear model in predicting torsional response of UTWRCMs.

2. Development of torsional equilibrium differential equation

A typical fixed-fixed UTWRCM subjected to a concentrated torque $T(l/2)$ applied at the mid-span is depicted in Fig. 1. The right-hand Cartesian coordinate system xoy is used in the derivation, where o is the centroid of member cross-section, x and y are the principal axes. When a UTWRCM is constrained at two ends, both circulatory torsion and warping torsion exist, as shown in Fig. 2. The applied torque $T(z)$ at any arbitrary location z is resisted by both circulatory torsion and warping torsion. The torsional equilibrium equation can thus be expressed as

$$T_c(z) + T_\omega(z) = T(z) \tag{1}$$

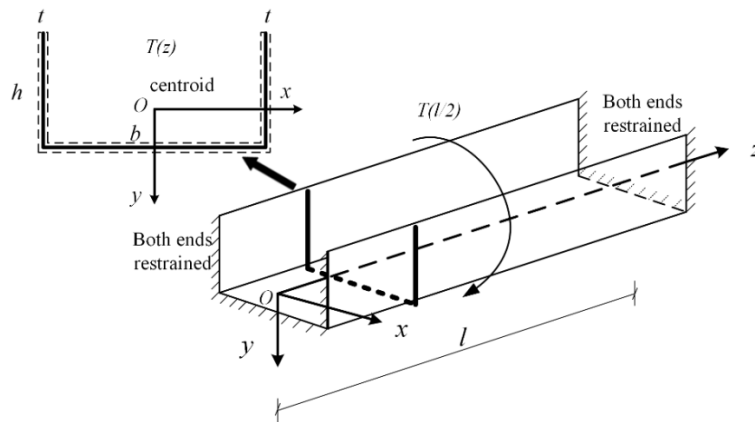


Fig. 1 Coordinate system and structural sketch of U-shaped thin-walled members in pure torsion

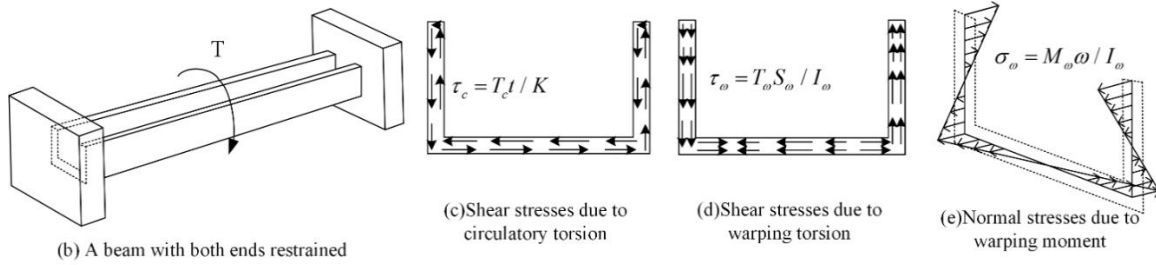


Fig. 2 Stress distribution along U-shaped cross sections

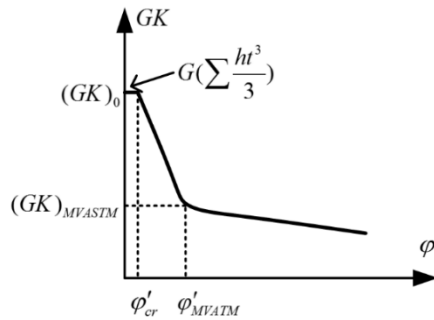


Fig. 3 Deterioration curve of circulatory torsional stiffness for U-shaped RC members

Where $T_c(z)$, $T_w(z)$ are respectively the torque induced by circulatory torsion and warping torsion at section z , and $T(z)$ is the applied torque at section z . For a fixed-fixed member with a concentrated torque T at the mid-span, $T(z)=T/2$.

2.1 Circulatory torsion

Circulatory torsion, which is also called the St.Venant torsion, can be obtained by

$$T_c = GK \cdot \varphi' \tag{2}$$

where GK is circulatory torsional stiffness, G is shear modulus of the material; K is the circulatory torsional constant, φ' is the first-order derivative of torsional rotation with respect to the coordinate z , i.e., the twist rate. If decompose the U-shaped section into n rectangles, $K = \sum \frac{h_i t_i^3}{3}$ in elastic stage, in which h_i and t_i are respectively the length and the width of the i^{th} rectangular component; Shear stresses (shown in Fig. 2(c)) corresponding to the circulatory torsion can be derived as

$$\tau_c = \frac{T_c}{K} t \tag{3}$$

Based on the softened space truss analogy model (Collins 1973, Hsu 1973, Hsu and Mo 2010, Bernardo, Andrade *et al.* 2012), the circulatory torsional stiffness over the entire loading process can be obtained. The modified variable angle truss model (MVATM) proposed by Bernardo, Andrade *et al.* (2012) is adopted in the current study to develop the post-cracking deteriorative curve of circulatory torsional stiffness. The U-shaped section is decomposed into three rectangular

sections, of which the circulatory torsional stiffness can be respectively obtained by MVATM. Resultant stiffness of the U-shaped section is the sum of the circulatory torsional stiffness of these three rectangular sections. The detailed procedures of computing the nonlinear circulatory torsional stiffness are summarized in (Bernardo, Andrade *et al.* 2012).

Fig. 3 displays the deterioration of the circulatory torsional stiffness GK of the U-shaped RC members with respect to the increase of its twist rate φ' determined by the MVATM. As can be seen from the figure, the circulatory torsional stiffness remains as a constant $((GK)_0)$ before cracking. Once crack appears, it reduces rapidly. The progress of the deterioration becomes much more slower when the member is fully cracked. This relation will be used in the following nonlinear analysis of UTWRCM torsional behavior.

2.2 Warping torsion and warping moment

Besides circulatory torsion, warping effects also plays an important role in the torsional behavior of open thin-walled members. Based on the Vlasov's theory (Vlasov 1984, Kollbrunner and Basler 2013), the torsion induced by elastic warping can be expressed in terms of sectorial coordinate as

$$T_\omega = -EI_\omega \cdot \varphi''' \tag{4}$$

where E is the elastic modulus of the material; I_ω is the principal sectorial moment of inertia; EI_ω is the warping torsional stiffness; $\omega = \int_s \rho ds$ is the sectorial area coordinate, where ρ is the polar radius with respect to the principle sectorial pole, and s is the coordinate in the curvilinear coordinate system; φ''' is the third-order derivative of torsional rotation with respect to the coordinate z . The elastic warping torsional stiffness $((EI_\omega)_0)$ shown in Fig. 4) can be evaluated by Vlasov's theory (Vlasov 1984, Kollbrunner and Basler 2013). Warping moment M_ω resulted from elastic warping can be obtained by integrating Eq. (4), which gives

$$M_\omega = -EI_\omega \varphi'' \tag{5}$$

where φ'' , the second-order derivative of the torsional rotation with respect to coordinate z , represents the curvature of deformation due to warping.

For any arbitrary cross section, the normal stress caused by warping moment and the shear stress caused by warping torsion (refer to Fig. 2) can be expressed respectively as

$$\sigma_\omega = \frac{M_\omega}{I_\omega} \omega \tag{6}$$

$$\tau_\omega = -\frac{T_\omega}{I_\omega} S_\omega \tag{7}$$

where $S_\omega = \int_A \omega dA$ is the sectorial static moment.

Although the warping torsional stiffness of an open thin-walled RC member in the elastic stage can be computed by applying Vlasov's theory, the approach to evaluate its value after concrete cracks is not yet available. In the current study, it is proposed to evaluate the post-cracking warping torsional stiffness of a RC member based on its equivalent section. The details of how to calculate the equivalent warping torsional stiffness in the post-cracking stage is described in the

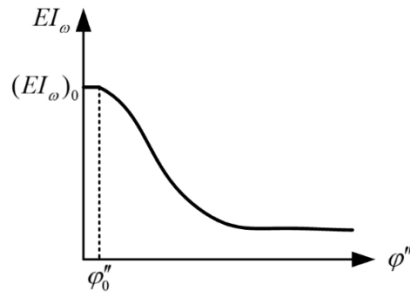


Fig. 4 Deterioration curve of warping torsional stiffness

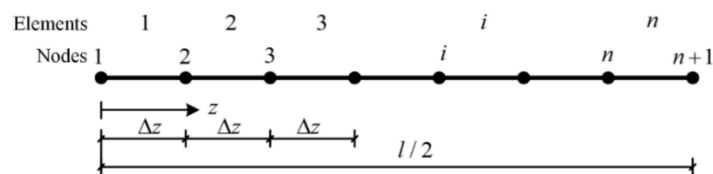


Fig. 5 Analysis element of U-shaped members

appendix. Fig. 4 depicts schematically the deterioration curve of the warping torsional stiffness of an UTWRCM with the increase of the curvature φ'' . As shown in Fig. 4, similar to the circulatory torsional stiffness, the warping torsional stiffness also remains unchanged before concrete cracks and drops rapidly with the formation of crack. It approaches to a constant value after the yielding of steel bars.

2.3 Differential equation for torque equilibrium

Substitute Eqs. (2) and (4) into Eq. (1), the differential equation for torque equilibrium can be achieved, i.e.

$$GK(z)\varphi'(z) - EI_{\omega}(z)\varphi'''(z) = T(z) \quad (8)$$

This third-order torque equilibrium differential equation can be solved using the fourth-order Runge-Kutta method.

3. Nonlinear model for predicting torsional response of UTWRCMs

3.1 Solution to torque equilibrium differential equation

Due to the symmetry of the studied UTWRCMs, only half of its span is considered in the analysis. As shown schematically in Fig. 5, the half-span of the UTWRCM is divided into n equal length segments along the z -axis by $(n+1)$ nodes. Each element has a length of Δz , $\Delta z = l/(2n)$, where l is the length of the UTWRCM. Assume Δz is infinitesimally small so that the associated element has uniform cross-sectional properties along its length. Take the i^{th} element as an example, both the circulatory torsional stiffness and the warping torsional stiffness of the element are assumed to be the same as those at node i . Further, it is assumed that the circulatory torsional

stiffness GK is not affected by the presence of warping flexural cracks and the warping torsional stiffness EI_ω is not influenced by the occurrence of circulatory torsional shear cracks. In other words, GK and EI_ω can be calculated independently without considering their interaction effect. Therefore, the circulatory torsional stiffness and warping torsional stiffness of the UTWRCM at each loading step can be computed respectively according to the MVATM (Bernardo, Andrade *et al.* 2012) and the equivalent warping torsional stiffness approach proposed in the current study.

Eq. (8) can be rewritten for the i^{th} element as

$$GK(\varphi'_i)\varphi'_i - EI_\omega(\varphi''_i)\varphi''_i = T\left(\frac{(i-1)l}{2n}\right) \tag{9}$$

The fourth-order Runge-Kutta method (McGuire, Gallagher *et al.* 2000) is applied to solve the above third-order differential equation, Denote $[\alpha_i \beta_i \gamma_i] = [\varphi_i \ \varphi'_i \ \varphi''_i]$, Eq. (9) can be expressed as

$$[\alpha'_i \ \beta'_i \ \gamma'_i]^T = \left[\beta_i \ \gamma_i \ \frac{GK(\beta_i)\beta_i - T\left(\frac{(i-1)l}{2n}\right)}{EI_\omega(\gamma_i)} \right]^T \tag{10}$$

To simplify this expression, define $f(\beta_i) = \beta_i$, $g(\gamma_i) = \gamma_i$ and $h(\beta_i, \gamma_i) = [GK(\beta_i)\beta_i - T\left(\frac{(i-1)l}{2n}\right)] / EI_\omega(\gamma_i)$. Thus, Eq.(10) can be rewritten as

$$[\alpha'_i \ \beta'_i \ \gamma'_i]^T = [f(\beta_i) \ g(\gamma_i) \ h(\beta_i, \gamma_i)]^T \tag{11}$$

Substituting the circulatory torsional stiffness ($GK(\beta_i)$) and the warping torsional stiffness ($EI(\gamma_i)$) corresponding to the i^{th} node into Eq.(11), the relation between the displacements at node i and node $(i+1)$ can be established as

$$\begin{bmatrix} \alpha_{i+1} \\ \beta_{i+1} \\ \gamma_{i+1} \end{bmatrix} = \begin{bmatrix} \alpha_i \\ \beta_i \\ \gamma_i \end{bmatrix} + \frac{\Delta z}{6} (\mathbf{k}_1 + 2\mathbf{k}_2 + 2\mathbf{k}_3 + \mathbf{k}_4) \tag{12}$$

where the vectors $\mathbf{k}_1, \mathbf{k}_2, \mathbf{k}_3, \mathbf{k}_4$ have the form of

$$\mathbf{k}_1 = \begin{bmatrix} k_{11} \\ k_{12} \\ k_{13} \end{bmatrix} = \begin{bmatrix} f(\beta_i) \\ g(\gamma_i) \\ h(\beta_i, \gamma_i) \end{bmatrix}; \quad \mathbf{k}_2 = \begin{bmatrix} k_{21} \\ k_{22} \\ k_{23} \end{bmatrix} = \begin{bmatrix} f(\beta_i + \Delta z \cdot k_{12} / 2) \\ g(\gamma_i + \Delta z \cdot k_{13} / 2) \\ h(\beta_i + \Delta z \cdot k_{12} / 2, \gamma_i + \Delta z \cdot k_{13} / 2) \end{bmatrix};$$

$$\mathbf{k}_3 = \begin{bmatrix} k_{31} \\ k_{32} \\ k_{33} \end{bmatrix} = \begin{bmatrix} f(\beta_i + \Delta z \cdot k_{22} / 2) \\ g(\gamma_i + \Delta z \cdot k_{23} / 2) \\ h(\beta_i + \Delta z \cdot k_{22} / 2, \gamma_i + \Delta z \cdot k_{23} / 2) \end{bmatrix};$$

$$\mathbf{k}_4 = \begin{bmatrix} k_{41} \\ k_{42} \\ k_{43} \end{bmatrix} = \begin{bmatrix} f(\beta_i + \Delta z \cdot k_{32} / 2) \\ g(\gamma_i + \Delta z \cdot k_{33} / 2) \\ h(\beta_i + \Delta z \cdot k_{32} / 2, \gamma_i + \Delta z \cdot k_{33} / 2) \end{bmatrix};$$

Apply the fixed boundary condition to node 1 at the support. At each loading step, the initial condition of node 1 is set as $[\alpha_1 \beta_1 \gamma_1]=[0 \ 0 \ \gamma_1]$, where γ_1 is determined based on the applied T at the corresponding loading step. Based on Vlasov’s elastic theory (Vlasov 1984), the initial value of γ_1 , i.e., φ_1'' can be derived by

$$\gamma_1 = \frac{T}{EI_\omega} \cdot \frac{1 - \cosh(\chi l / 2)}{\chi \sinh(\chi l / 2)} \tag{13}$$

where $\chi = \sqrt{GK / EI_\omega}$ is the ratio between the circulatory torsional stiffness and the warping torsional stiffness. Eq. (13) is not applicable after concrete cracks because both circulatory and warping torsional stiffness would vary along the member length. Therefore, the average value of these two kinds of torsional stiffness, as given in Eq. (14) and (15), are substituted into Eq. (13) for computing the stiffness ratio χ in the post-cracking stage.

$$\overline{GK} = \sum_{i=1}^n GK(\beta_i) / n \tag{14}$$

$$\overline{EI_\omega} = \sum_{i=1}^n EI_\omega(\gamma_i) / n \tag{15}$$

Finally, the displacement vector at all the nodes can be evaluated using Eq. (12). By gradually increasing the applied torque, the torsional response of the studied UTWRCM over the entire loading process can be calculated.

3.2 Refinement of torsional rotation by considering warping shear deformation

When Vlasov’s elastic theory was applied to derive the torque equilibrium differential equation, Eq. (16), for open thin-walled members under pure torsion, it was assumed that no shear deformation would occur at the midline of any arbitrary section. This assumption is valid in the elastic range. However, after concrete cracks, the effect of shear deformation on the torsional response of the member cannot be ignored. It was reported in literature (Krpan and Collins 1981a, Luccioni, Reimundin *et al.* 1996, Pavazza 2005) that although the shear stress caused by warping torsion would not affect the shear bearing capacity, it would considerably increase the torsional rotation of the member. Data obtained from an experimental study by Krpan and Collins (1981a) indicated that more than 60% of the torsional rotation was induced by shear strain after the

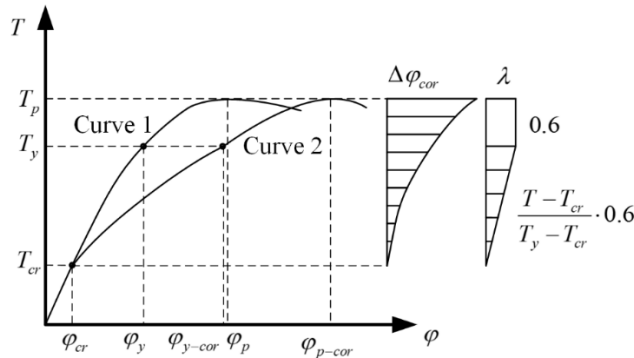


Fig. 6 Refinement of the torque- rotation curve

yielding of steel bars. In the current study, the effect of shear deformation on the bearing capacity of UTWRCMs under pure torsion will be neglected. The Refinement of the member torsional rotation will be achieved based on Eq. (17), i.e.

$$\varphi_{cor} = \varphi + \Delta\varphi_{cor} = \varphi + \lambda \cdot \varphi \quad (18)$$

Where φ_{cor} is the refined torsional rotation with the consideration of warping shear deformation; φ is the torsional rotation; $\Delta\varphi_{cor}$ is the amount of applied correction to the torsional rotation; and λ is the empirical amplification coefficient. As is shown in Fig. 6, the torque-rotation curve can be divided into three stages by two characteristic points, i.e., the diagonal shear cracking point (T_{cr}) and the longitudinal bar yielding point (T_y).

The empirical amplification coefficient λ is determined based on the magnitude of the applied torque T :

- (1) Prior to the occurrence of diagonal shear cracks ($T \leq T_{cr}$): $\lambda=0$, which neglects the effect of

shear deformation.

- (2) From the occurrence of diagonal shear cracks till yielding of the longitudinal bars ($T_{cr} < T < T_y$): Assume the torsional rotation induced by warping shear deformation has a linear relation with the increase of the applied torque, i.e.

$$\lambda = \frac{0.6}{T_y - T_{cr}} \cdot (T - T_{cr}) \quad (19)$$

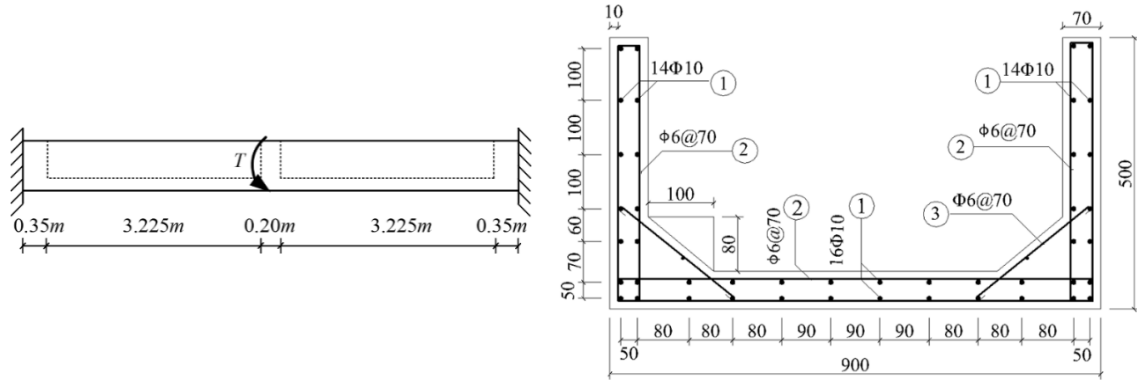
- (3) After yielding of the longitudinal bars ($T_y \geq T$): $\lambda=0.6$.

A refined torque-rotation curve describing the torsional response of UTWRCMs over the entire loading process can be obtained by applying the above correction to the torsional rotation in the post-cracking stage. Curve 1 and 2 in Fig. 6 portray respectively the torque-rotation curves without and with the refinement.

4. Application of the proposed nonlinear model

4.1 Description of specimens used in existing experimental studies

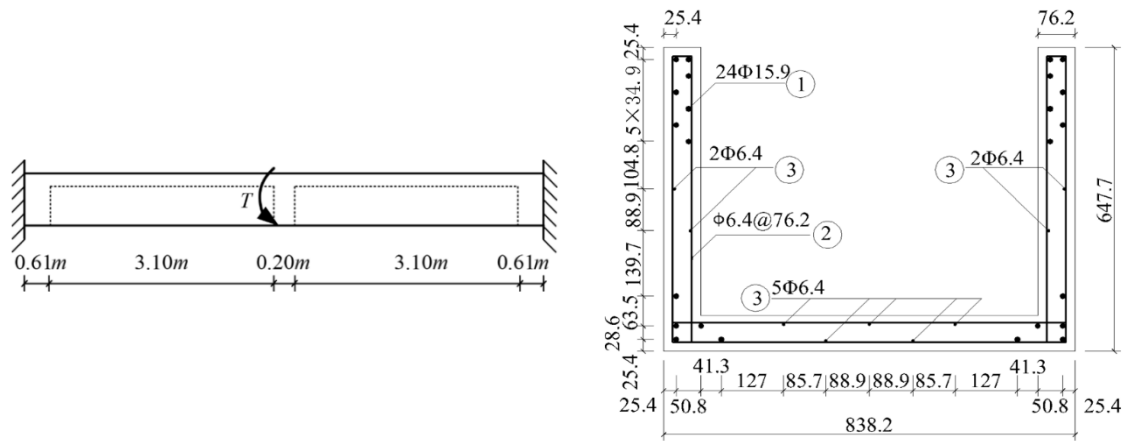
The torsional response of five UTWRCM specimens, four tested recently by our research group (Chen, Diao *et al.* 2016) and another one by Krpan and Collins in 1981 (Krpan and Collins 1981b), are analyzed in this section using the proposed nonlinear model. The results are then compared with the existing experimental data. The four specimens tested in (Chen, Diao *et al.* 2016) are denoted as MEM-1, MEM-2, MEM-3 MEM-4, whereas the one tested in (Krpan and Collins 1981b) is denoted as MEM-C. Detailed dimensions and reinforcement arrangement of these five specimens are given in Fig. 7 and Fig. 8. The only difference between the four specimens tested in (Chen, Diao *et al.* 2016) is that the diameter of the longitudinal steel bars in MEM-1 and MEM-2 is 10mm, whereas the diameter of those in MEM-3 and MEM-4 is 8mm. The mechanical and material properties of all the specimens are listed in Table 1. For other related information, please refer to (Krpan and Collins 1981b, Chen, Diao *et al.* 2016).



(a) Dimensions of tested specimen MEM-1

(b) Reinforcement of tested specimen MEM-1

Fig. 7 Details of tested specimen MEM-1



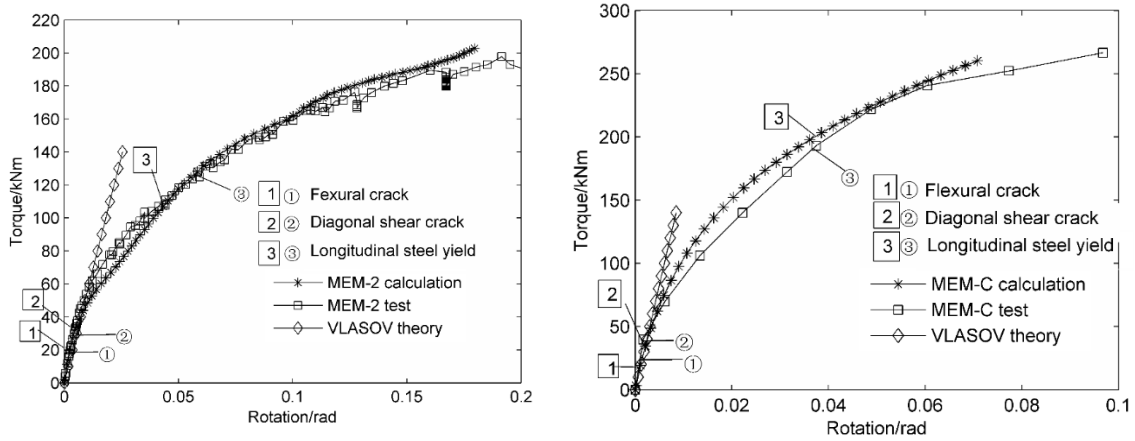
(a) Dimensions of tested specimen MEM-C

(b) Reinforcement of tested specimen MEM-C

Fig. 8 Details of specimen MEM-C

Table 1 Mechanical properties of specimens

Material	Specimen	MEM-1	MEM-2	MEM-3	MEM-4	MEM-C
Concrete	Compressive strength of cube specimen (MPa)	50.95	50.95	63.83	51.57	52.00
	Elastic modulus (GPa)	40.00	38.50	42.20	34.38	34.04
Longitudinal Steel bar	Reinforcement ratio (%)	2.80	2.80	1.80	1.80	3.16
	Diameter (mm)	10	10	8	8	15.9
	Yield strength (Mpa)	576.25	576.25	353.33	353.33	348
	Ultimate strength (Mpa)	623.00	623.00	573.33	573.33	475
Stirrup	Diameter (mm)	6	6	6	6	6.4
	Yield strength (Mpa)	365.00	365.00	276.70	276.70	362.00
	Ultimate strength (Mpa)	645.00	645.00	446.70	446.70	492.60



(a) Torque-rotation curves of specimen MEM-2 (b) Torque-rotation curves of specimen MEM-C

Fig. 9 Comparison of analytically predicted and experimentally recorded torque-rotation curves

4.2 Torque-rotation curves

The proposed nonlinear model is applied to determine the torsional response of the five UTWRCM specimens under pure torsion. Fig. 9 illustrates the torque-rotation curves associated with two sample specimens MEM-2 and MEM-C. In each case, besides the theoretical prediction and experimental data, the variation of torsional rotation with respect to the applied torque determined based on Vlasov’s elastic model is also shown in the figure for convenience of comparison. Results show that for both specimens, prior to formation of the diagonal shear cracks, the torque-rotation curves obtained from three different approaches agree well with each other. However, once the diagonal shear crack forms, the results obtained from Vlasov’s elastic model deviate considerably from the other two sets because of significant reduction in the member torsional stiffness, whereas the prediction based on the proposed nonlinear model remains comparing well with the experimental data for the rest of the loading history. This clearly indicates that Vlasov’s elastic theory is applicable to determine the response of open thin-walled RC members under pure torsion in the elastic stage, whereas the proposed nonlinear model is capable of predicting its behavior over the entire loading process.

4.3 Cracking torque and yielding torque

Three characteristic points, namely the flexural cracking point, the web shear cracking point and the yielding point, are shown on the torque-rotation curves in Fig. 9. They divide the entire loading process of the studied UTWRCMs into three stages. Based on experimental observation and mechanical analysis, two types of cracks, i.e., vertical flexural cracks and diagonal web shear cracks, are identified. The initiation of the vertical flexural crack is dictated by the magnitude of the normal stress due to warping moment at the support or mid-span sections. The normal tensile stress caused by warping moment can be computed using Eq. (6). Once it exceeds the concrete tensile strength, which is $0.63\sqrt{f'_c}$ (MPa) according to ACI 318-05, where f'_c is the concrete compressive strength measured by the standard cylinder test, the first ‘vertical flexural crack’

Table 2 Comparison of experimentally obtained and theoretically predicted torques (k·Nm)

Specimen	Cracking torque						Yielding torque			Ultimate torque		
	Flexural cracking			Web shear cracking			T_{test}^a	T_{cal}	T_{test}/T_{cal}	T_{test}	T_{cal}	T_{test}/T_{cal}
	T_{test}	T_{cal}	T_{test}/T_{cal}	T_{test}	T_{cal}	T_{test}/T_{cal}						
MEM-1	20.00	20.40	0.98	36.00	32.00	1.12	—	138.5	—	—	206.1	—
MEM-2	22.00	20.40	1.08	36.00	32.00	1.13	114.9	138.5	0.83	199.7	206.1	0.97
MEM-3	19.30	18.10	1.07	36.00	36.10	1.00	87.50	89.80	0.97	151.0	147.2	1.03
MEM-4	17.29	17.78	0.97	56.00	35.40	1.58	90.00	89.80	1.00	147.0	147.2	0.99
MEM-C	23.00	18.10	1.27	39.00	36.30	1.07	191.0	200.4	0.95	266.0	259.4	1.03
	$X_{average} =$		1.07	$X_{average} =$		1.18	$X_{average} =$		0.94	$X_{average} =$		1.01
	$SD =$		0.07	$SD =$		0.20	$SD =$		0.06	$SD =$		0.02
	$CV =$		6.5%	$CV =$		17%	$CV =$		6.8%	$CV =$		2.7%

Note: T_{test} =tested value; T_{cal} =calculated value; $X_{average}$ =average value of T_{test}/T_{cal} ; SD =sample standard deviation; CV =coefficient of variation.

^aTested values of yielding torque is the average values of the first yielding in reference (Chen, Diao *et al.* 2016).

would appear. The shear stress contains two components, one resulted from the circulatory torsion and the other from the warping torsion. They can be determined based on Eqs. (3) and (7), respectively. Similarly, once the maximum resultant shear stress reaches the concrete shear strength, i.e., $0.33\sqrt{f'_c}$ (MPa), the first diagonal shear crack will appear at a quarter span.

The torques at the three characteristic points are predicted for the five UTWRCM specimens by applying the proposed nonlinear model. They are summarized in Table 2, together with those measured in the experimental tests. The theoretically predicted and experimentally measured torsional rotation corresponding to the three characteristic points are listed in Table 3. It is worth mentioning that limited by the capacity of the originally selected actuator, the loads applied to MEM-1 did not reach the ultimate value (Chen, Diao *et al.* 2016). Consequently, data collected for MEM-1 were not complete. As can be seen from Table 2, for the five studied specimens, the predicted vertical flexural cracking torque, yielding torque and ultimate torque agree well with the experimental data, with an average ratio between the experimental data and the theoretical prediction being respectively 1.07, 1.01 and 1.01, and the associated coefficient of variation being 6.5%, 7.1% and 2.7%, respectively. However, the predicted torque corresponding to the occurrence of the diagonal web shear crack has a relatively large discrepancy when compared to the experimental results. The average ratio between the two sets is $X_{average}=1.18$, and the coefficient of variation is 17%. A closer look at the results in Table 2 reveals that this relatively large discrepancy is mainly due to the great delay of diagonal web shear crack formation in MEM-4. However, although the proposed nonlinear model can properly predict the torsional rotation at the formation of the vertical flexural crack and the diagonal web shear crack with $X_{average}$ being respectively 0.96 and 0.892, large dispersion exists for $\varphi_{test}/\varphi_{cal}$, which is 17.3% and 19.7%, respectively. Further, the predicted torsional rotation at the yielding of longitudinal reinforcement is significantly larger than that recorded in the test, with $X_{average}=0.70$ and the coefficient of variation being 26.4%. Therefore, more research effort is needed to improve the prediction of torsional rotation.

Table 3 Comparison of experimentally obtained and theoretically predicted torsional rotation (rad)

Specimen	Rotation at cracking						Rotation at yielding		
	Flexural cracking			Web shear cracking			φ_{test}	φ_{cal}	$\varphi_{test}/\varphi_{cal}$
	φ_{test}	φ_{cal}	$\varphi_{test}/\varphi_{cal}$	φ_{test}	φ_{cal}	$\varphi_{test}/\varphi_{cal}$			
MEM-1	0.0022	0.0025	0.88	0.0047	0.0048	0.98	—	0.0656	—
MEM-2	0.0030	0.0025	1.20	0.0046	0.0048	0.96	0.0476	0.0656	0.73
MEM-3	0.0016	0.0021	0.76	0.0040	0.0064	0.63	0.0215	0.0458	0.57
MEM-4	0.0017	0.0020	0.85	0.0070	0.0062	1.13	0.0230	0.0458	0.50
MEM-C	0.0010	0.0009	1.11	0.0016	0.0021	0.76	0.0368	0.0373	0.98
	$X_{average} =$		0.960	$X_{average} =$		0.892	$X_{average} =$		0.70
	SD =		0.166	SD =		0.176	SD =		0.185
	CV =		17.3%	CV =		19.7%	CV =		26.4%

Note: φ_{test} =tested rotation; φ_{cal} =calculated rotation; $X_{average}$ = average value of of $\varphi_{test}/\varphi_{cal}$; SD=sample standard deviation; CV=coefficient of variation.

^aTested values of rotation at yielding is the average value of rotations corresponding to the first yielding in reference (Chen, Diao *et al.* 2016).

4.4 Effect of warping torsion

Torsion in open thin-walled members consists of both circulatory torsion and warping torsion. They cannot be isolated in the experimental test and measured separately. Therefore, it is difficult to directly obtain the effect of warping on the torsional response of UTWRCMs from the testing data. To better understand the impact of warping on the torsional response of an open thin-walled members, analysis will be performed in this section based on the proposed concept of equivalent warping torsional stiffness in the post-cracking stage.

4.4.1 Deterioration of warping torsional stiffness

An approach to compute the warping torsional stiffness of an open thin-walled member having an arbitrary cross-section in pure torsion is illustrated in the appendix. It is applied to determine the warping torsional stiffness deterioration curve for MEM-2, MEM-3 and MEM-C, as portrayed in Fig. 10. Results show that prior to concrete cracking (point ① in Fig.10), the warping torsional stiffness of a UTWRCM remains as a constant. With the formation of cracks, concrete in tension zone no longer contributes to the resistance, which leads to a significant reduction in the warping torsional stiffness. In other words, the concrete cracking point, point ①, is a key point which indicates the beginning of deterioration in the warping torsional stiffness. When the longitudinal bar yields (point ② in Fig. 10), the warping torsional stiffness of the three studied specimens is reduced respectively by 75.3%, 76.1%, and 45.5% of their initial values. It is interesting to note that in the case of MEM-C, the reduction of warping torsional stiffness between point ① and point ② is much less than that in the other two specimens. This is mainly because the longitudinal bars in MEM-C exhibits a more obvious and wider yielding stage. The warping torsional stiffness of this specimen continuously drop beyond the yielding point at a relatively slower rate. However, in

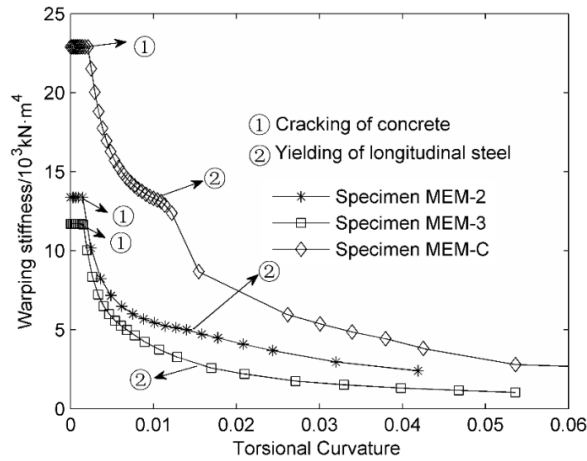


Fig. 10 Calculated deterioration curves of warping torsional stiffness

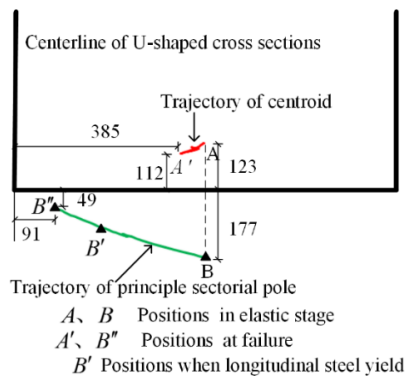


Fig. 11 Calculated trajectory of principal sectorial pole (unit: mm)

the case of MEM-2 and MEM-3, after the longitudinal reinforcements yields, with the rapid growth of the member curvature (φ''), there is a much less reduction in the warping torsional stiffness.

4.4.2 Warping property of a U-shaped cross section

Warping effect has a visible impact on the torsional property of UTWRCMs, especially in the inelastic stage. After concrete cracks, the warping torsional stiffness of the members constantly varies. Fig. 11 describes the variation of the cross-sectional properties of MEM-3 over the entire loading process. Point A and point B represent respectively the original position of the centroid and principle sectorial pole (i.e., center of twist) of the U-shaped cross section. They remain unchanged prior to the formation of the vertical flexural cracks. After concrete cracks, concrete in tension zone no longer contributes to resistance and longitudinal reinforcement would carry all tensile stress. Changes of strain condition of this cross section due to warping lead to the position changes of the centroid and the principle sectorial pole. As can be seen from Fig. 11, when the specimen failed, the position of centroid moved from point A to point A', whereas that of the principle pole moved from point B to point B''. Over the entire loading process, the position of the

principle sectorial pole shifted significantly by -324 mm and -128 mm along the x -axis and the y -axis, respectively, where the negative sign represents the direction of movement is opposite to the positive direction of the coordinate axes defined in Fig. 1.

The change in position of the principle sectorial pole would affect the principle sectorial area coordinates ω and the principal sectorial static moment S_ω , which, based on Eqs. (6) and (7), are directly related to the warping normal stress and warping shear stress. The distribution of ω and S_ω over the member cross section in the elastic stage, at the yielding of the longitudinal reinforcements and the member failure are given respectively in the three subplots in Fig. 12. Compared to Fig. 12(a), the distribution of the principle sectorial area ω in the post-cracking stage is no longer anti-symmetric, as can be seen from Figs. 12 (b) and (c). With the increase of the applied torque, the neutral axis, represented by the dashed line in Fig. 12, shifts towards the compression zone (denoted by the positive sign in Fig. 12). This results in a gradual reduction of the compression zone but expansion of the tension zone. When the ultimate torque is reached, the stress condition of the two flanges differs considerably. The compression zone in the left flange almost vanishes, whereas its maximum tensile stress is significantly higher than that in the right flange. In addition, the principle sectorial static moment S_ω is found to decrease with the increase of the applied torque. At failure, it drops to less than 20% of its value in the elastic stage, which

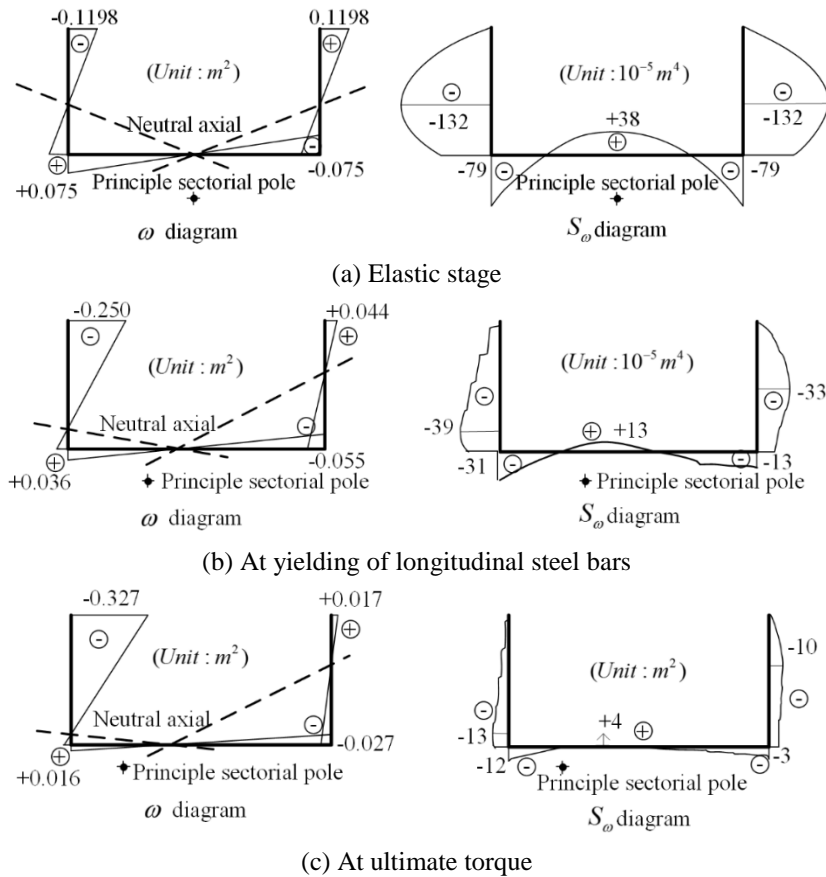


Fig. 12 Distribution of ω and S_ω over the mid-span section of a U-shaped RC member

suggests that the warping shear stress plays a minor role in the post-cracking stage. This agrees with the observation reported in (Chen, Diao *et al.* 2016) that after yielding, further development of the diagonal shear crack was dictated by the circulatory torsional shear stress.

5. Conclusions

A nonlinear model has been proposed in the current study to predict torsional behavior of U-shaped thin-walled RC members under pure torsion. It has been applied to analyze torsional response of five UTWRCMs experimentally tested in the literature. The following conclusions are drawn based on the comparison between the theoretical prediction and the existing experimental data.

- The proposed nonlinear model can effectively predict the torsional behavior of UTWRCMs over the entire loading process. The prediction by the proposed model agrees well with the existing experimental data.
- The key issue is to determine the deterioration curves of the circulatory torsional stiffness and the warping torsional stiffness. While the circulatory torsional stiffness can be determined by the existing theory of MVATM, the warping torsional stiffness deterioration curve of UTWRCMs over the entire loading history can be computed by introducing the concept of equivalent warping torsional stiffness in the post-cracking stage.
- The effect of shear deformation due to warping torsion on the post-cracking torsional rotation of UTWRCMs cannot be ignored in the analysis. The introduction of an empirical modification factor would allow effectively estimating the additional rotation caused by warping shear deformation.

Acknowledgements

This work is part of the projects financially supported by the Natural Science Fund (NSF) of China Grant No. 51278020 and the Fund of State Key Laboratory of Subtropical Building Science (FSKLSBS) South China University of Technology Grant No. 2015ZA03. Authors gratefully acknowledge the funding from the NSF and FSKLSBS.

References

- Aminbaghai, M., Murin, J., Hrabovsky, J. and Mang, H.A. (2016), "Torsional warping eigenmodes including the effect of the secondary torsion moment on the deformations", *Eng. Struct.*, **106**, 299-316.
- Bernardo, L., Andrade, J. and Lopes, S. (2012), "Modified variable angle truss-model for torsion in reinforced concrete beams", *Mater. Struct.*, **45**(12), 1877-1902.
- Bernardo, L.F.A., Andrade, J.M.A. and Nunes, N.C.G. (2015), "Generalized softened variable angle truss-model for reinforced concrete beams under torsion", *Materials and Structures*, **48**(7), 2169-2193.
- Chen, S., Diao, B., Guo, Q., Cheng, S. and Ye, Y. (2016), "Experiments and calculation of U-shaped thin-walled RC members under pure torsion", *Eng. Struct.*, **106**, 1-14.
- Collins, M.P. (1973), "Torque-twist characteristics of reinforced concrete beams", *Inelast. Nonlin. Struct. Concrete*, 211-231.
- Erkmen, R.E. and Mohareb, M. (2006), "Torsion analysis of thin-walled beams including shear deformation

- effects”, *Thin Wall. Struct.*, **44**(10), 1096-1108.
- Hsu, T.T. (1973). “Post-cracking torsional rigidity of reinforced concrete sections”, *ACI J. Proc.*, **70**(5), 352-360.
- Hsu, T.T. and Mo, Y.L. (2010), *Unified Theory of Concrete Structures*, John Wiley & Sons.
- Hwang, C.S. and Hsu, T.T. (1983). “Mixed torsion analysis of reinforced concrete channel beams—a fourier series approach”, *ACI J. Proc.*, **80**(5), 377-386.
- Jeng, C.H. and Hsu, T.T. (2009), “A softened membrane model for torsion in reinforced concrete members”, *Eng. Struct.*, **31**(9), 1944-1954.
- Kollbrunner, C.F. and Basler, K. (2013), *Torsion in Structures: an Engineering Approach*, Springer Science & Business Media.
- Krpan, P. and Collins, M.P. (1981a), “Predicting torsional response of thin-walled open RC members”, *J. Struct. Div.*, **107**(6), 1107-1127.
- Krpan, P. and Collins, M.P. (1981b), “Testing thin-walled open RC structure in torsion”, *J. Struct. Div.*, **107**(6), 1129-1140.
- Luccioni, B., Reimundin, J. and Danesi, R. (1991). “Prestressed concrete I-beams under combined mixed torsion, flexure and shear”, *ICE Proc.*, **91**(3), 577-592.
- Luccioni, B.M., Reimund, J.C. and Danesi, R. (1996), “Thin-walled prestressed concrete members under combined loading”, *J. Struct. Eng.*, **122**(3), 291-297.
- McGuire, W., Gallagher, R.H. and Ziemian, R.D. (2000), *Matrix Structural Analysis*.
- Murín, J. and Kutiš, V. (2008), “An effective finite element for torsion of constant cross-sections including warping with secondary torsion moment deformation effect”, *Eng. Struct.*, **30**(10), 2716-2723.
- Pavazza, R. (2005), “Torsion of thin-walled beams of open cross-section with influence of shear”, *Int. J. Mech. Sci.*, **47**(7), 1099-1122.
- Timoshenko, S.P. (1945), “Theory of bending, torsion and buckling of thin-walled members of open cross section”, *J. Franklin Inst.*, **239**(4), 249-268.
- Vlasov, V.Z. (1984), *Thin-walled elastic beams*, National Technical Information Service.
- Waldron, P. (1986), “Sectorial properties of straight thin-walled beams”, *Comput. Struct.*, **24**(1), 147-156.
- Zbirohowski-Koscia, K. (1968), “Stress analysis of cracked reinforced and prestressed concrete thin-walled beams and shells”, *Mag. Concrete Res.*, **20**(65), 213-220.

PL

Nomenclature

A	cross-sectional area;
A_s, A_c	the actual area of steel bars and concrete section;
A'_s, A'_c	the equivalent area of steel bars and concrete section;
C	a constant of integration;
E	elastic modulus of material;
E_0	the initial elastic modulus of concrete;
E_s, E_c	secant modulus of steel bars and concrete;
f'_c	concrete compressive strength measured by the standard cylinder test;
f_y, f_p	yielding strength and ultimate strength of steel bars;
$f(\beta), g(\gamma), h(\beta, \gamma)$	expressions to simplify the expression;
G	shear modulus of material;
h	height of a cross section;
i	numbering of each element;

I_x, I_y	moment of inertia about axis x or y , respectively;
I_{xy}	product of inertia;
I_ω	principle sectorial moment of inertia;
$I_{\omega_A x}, I_{\omega_A y}$	sectorial linear static moment about axis x or y , respectively;
K	circulatory torsional constant;
$\mathbf{k}_1, \mathbf{k}_2, \mathbf{k}_3, \mathbf{k}_4$	state vectors;
l	beam span;
M_ω	warping moment;
m_1	an initial variable determined by the loading level;
n	total number of element segments;
s	curvilinear coordinate;
S	static moment;
SS_x, SS_y	interim parameters in applying Simpson's rule;
S_ω	sectorial static moment;
T	total applied torque;
T_c	circulatory torsion;
T_{cr}	diagonal shear cracking torque;
T_y	yielding torque of longitudinal steel bars;
$T(z)$	applied torque at section z ;
T_ω	warping torsion;
t	shorter dimension of a cross section;
(X, Y)	coordinates in a coordinate system with an arbitrary origin;
x, y, z	centroidal principle axes;
(x_A, y_A)	coordinates of center of gravity;
(x_B, y_B)	coordinates of principle sectorial pole;
α, β, γ	simplified symbols for expressing terms φ, φ' and φ'' ;
ε	longitudinal strain;
ε_0	strain of concrete corresponding to peak compressive stress;
ε_u	ultimate strain of compressive concrete;
$\varepsilon_y, \varepsilon_p$	strains of steel bars corresponding to yielding and ultimate loads, respectively;
φ	torsional rotation;
φ'	the first-order derivative of torsional rotation with respect to coordinate z ;
φ''	the second-order derivative of torsional rotation with respect to coordinate z ;
φ'''	the third-order derivative of torsional rotation with respect to coordinate z ;
φ_{cor}	torsional rotation after correction;
χ	ratio between the circulatory torsional stiffness and the warping torsional stiffness;
λ	empirical correction coefficient;
ρ	polar radius with respect to principle sectorial pole;
ρ_A, ρ_B	polar radius with respect to point A and point B, respectively;
σ_ω	warping normal stress;
ω	sectorial area coordinate;
τ_c	circulatory shear stress;
τ_ω	warping shear stress;
$\Delta\varphi_{cor}$	modified variation of torsional rotation;
ΔA	area of a differential segment;

Appendix A. Approach to determine warping torsional stiffness of open thin-walled RC members with arbitrary cross section

A.1 Location of principle sectorial pole

A principle sectorial coordinate system needs to be established to analyze the warping properties of open thin-walled members (Vlasov 1984, Kollbrunner and Basler 2013). The origin of this coordinate system is defined as the principle sectorial pole, i.e., the center of twist. If apply a torque at this point, no axial force and bending moment will be induced. This condition can be mathematically expressed as

$$\begin{cases} \int_A \omega dA = 0 \\ \int_A \omega y dA = 0 \\ \int_A \omega x dA = 0 \end{cases} \quad (20)$$

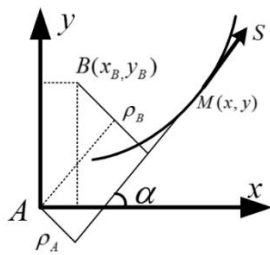


Fig. A1 Coordinate systems

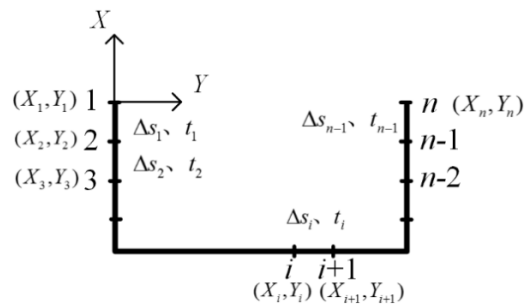


Fig. A2 Segments of a typical U-shaped cross section

Fig. A1 shows an infinitesimal element of an open thin-walled cross section. A Cartesian coordinate system xoy is established, the origin of which is set at the centroid of the section, i.e., point A in Fig. A1. Besides, a curvilinear coordinate s is introduced which is along the midline of the sections. Assume point B is the actual principle sectorial pole. Based on the definition of the sectorial area coordinate, the differential sectorial area coordinate at point $M(x,y)$ by respectively taking point A and point B as the sectorial pole are

$$d\omega_A = \rho_A ds = (x \sin \alpha - y \cos \alpha) ds = x dy - y dx \quad (21)$$

$$d\omega_B = \rho_B ds = (\rho_A - x_B \sin \alpha + y_B \cos \alpha) ds = d\omega_A - x_B dy + y_B dx \quad (22)$$

where ρ_A, ρ_B are the polar radius with respect to point A and point B, respectively; $\sin \alpha = dy/ds$ and $\cos \alpha = dx/ds$. Integrate Eq. (22) along s gives

$$\omega_B = \omega_A - x_B y + y_B x + C \quad (23)$$

where C is the integration constant.

Substitute Eq. (23) into Eq. (20), the coordinates of point B in the Cartesian coordinate system

and the integration constant can be expressed as

$$\begin{cases} x_B = \frac{I_y I_{\omega_A x} - I_{xy} I_{\omega_A y}}{I_x I_y - I_{xy}^2} \\ y_B = -\frac{I_x I_{\omega_A y} - I_{xy} I_{\omega_A x}}{I_x I_y - I_{xy}^2} \\ C = -\frac{S_{\omega_A}}{A} \end{cases} \quad (24)$$

where A is the cross sectional area; $I_x = \int_A y^2 dA$, $I_y = \int_A x^2 dA$ are the moment of inertia referring respectively to the x -axis and y -axis; $I_{xy} = \int_A xy dA$ is the product of inertia; $I_{\omega_A x} = \int_A \omega_A y dA$, $I_{\omega_A y} = \int_A \omega_A x dA$ are the sectorial linear static moment referring respectively to x -axis and y -axis.

A.2 Warping torsional stiffness in the elastic stage

The approach proposed here for calculating the sectorial properties of an open thin-walled section is applicable to any arbitrary cross-sectional shape. Since the U-shaped section is the focus of the current study, it will be used as an example to illustrate the procedures of the proposed approach. As the first step, a Cartesian coordinate system is established by taking the top point of the left flange as the origin, as shown in Fig. A2. Then, the entire cross section is divided into $(n-1)$ segments by n nodes. The length of the segments should be short enough to ensure the thickness within each element is a constant. For the i^{th} segment with the thickness t_i , its area can be calculated by

$$\Delta A_i = t_i \cdot \sqrt{(X_{i+1} - X_i)^2 + (Y_{i+1} - Y_i)^2} \quad (25)$$

where (X_i, Y_i) and (X_{i+1}, Y_{i+1}) are the coordinates of node i and node $i+1$. Transforming the coordinate of node i to a Cartesian coordinate system with the origin at the centroid of the cross section, it gives

$$\begin{cases} x_i = X_i - \frac{\int_A X dA}{\int_A dA} = X_i - \frac{\sum \Delta A_i \cdot \frac{1}{2}(X_i + X_{i+1})}{\sum \Delta A_i} \\ y_i = Y_i - \frac{\int_A Y dA}{\int_A dA} = Y_i - \frac{\sum \Delta A_i \cdot \frac{1}{2}(Y_i + Y_{i+1})}{\sum \Delta A_i} \end{cases} \quad (26)$$

Next, the sectorial properties of the section are calculated using the incremental method. The increment of the sectorial area coordinate between the two adjacent nodes based on sectorial pole A can be derived using Eq. (21), i.e.

$$\Delta \omega_{Ai} = x_i \Delta y_i - y_i \Delta x_i = x_i y_{i+1} - y_i x_{i+1} \quad (27)$$

The increment of static moment are obtained by

$$\begin{cases} \Delta S_{x,i} = \Delta A_i (y_{i+1} + y_i) / 2 \\ \Delta S_{y,i} = \Delta A_i (x_{i+1} + x_i) / 2 \end{cases} \quad (28)$$

Since in the case of an open section, the static moment at the open edges of the section equals to zero, i.e., $S_1=S_n=0$. They can be used respectively as the initial condition for node 1 and the final check of S_n for node n .

In terms of the moment of inertia, they can be calculated by integrating the static moment over the entire cross section. For the i^{th} segment, the static moment of node i , node $i+1$ and the segment middle node $\text{mid-}i$ can all be computed following the above procedures. The interim parameters of SS_{xi} and SS_{yi} for the i^{th} segment can thus be computed from

$$\begin{cases} SS_{x,i} = S_{x,i} + 4S_{x,\text{mid-}i} + S_{x,i+1} \\ SS_{y,i} = S_{y,i} + 4S_{y,\text{mid-}i} + S_{y,i+1} \end{cases} \quad (29)$$

Applying the Simpson’s rule, the moment of inertia and the sectorial moment of inertia can be evaluated by the following equations

$$\begin{cases} I_x = -\sum SS_{y,i} \cdot \Delta y_i / 6 \\ I_y = -\sum SS_{x,i} \cdot \Delta x_i / 6 \\ I_{xy} = -\sum SS_{y,i} \cdot \Delta x_i / 6 \end{cases} \quad (30)$$

$$\begin{cases} I_{\omega_A x} = -\sum SS_{y,i} \cdot \Delta \omega_{Ai} / 6 \\ I_{\omega_A y} = -\sum SS_{x,i} \cdot \Delta \omega_{Ai} / 6 \end{cases} \quad (31)$$

Substitute the values of moment of inertia determined by Eqs. (30) and (31) into Eq. (24). It yields the coordinates of the actual principle sectorial pole (x_B, y_B) . Apply Eq. (23), the sectorial coordinates of a node can be transformed from that based on the principle pole at point A (i.e., ω_A) to that based on the actual principle sectorial pole at point B (i.e. ω_B). Once the principle sectorial coordinates is obtained, the corresponding warping parameters, i.e. principle sectorial static moment S_ω and the principle sectorial moment of inertia I_ω , can be conveniently determined. Finally, the warping torsional stiffness of the section in the elastic stage can be obtained as the product of I_ω and the elastic modulus E .

A.3 Warping torsional stiffness in the post-cracking stage

After concrete cracks, the behavior of concrete and reinforcing bars in a reinforced concrete member needs to be considered independently by applying their respective constitutive relations. For the convenience of analysis, it is assumed to introduce an imaginary new material of which its elastic modulus is the same as the initial elastic modulus of concrete E_0 . Based on the equivalent area method, the area of the concrete or the reinforcement at a specific stress level in the i^{th} segment can be transformed into the equivalent area of the new material at the same stress level by

$$\begin{cases} A_{si}' = \frac{E_{si}}{E_0} A_{si} \\ A_{ci}' = \frac{E_{ci}}{E_0} (A_{ci} - A_{si}) \end{cases} \quad (32)$$

where A_{si}' , A_{si} are respectively the transformed equivalent area and the original actual area of steel reinforcement in the i^{th} segment; A_{ci}' , A_{ci} are respectively the transformed equivalent area and the original actual area of concrete in the i^{th} segment; E_{si} , E_{ci} are the secant modulus of steel reinforcement and concrete at a specific stress level in the i^{th} segment, respectively.

Substitute Eq. (25) into Eq. (32), the transformed equivalent area of an arbitrary segment i can be obtained as

$$\Delta A_i = A_{si}' + A_{ci}' \quad (33)$$

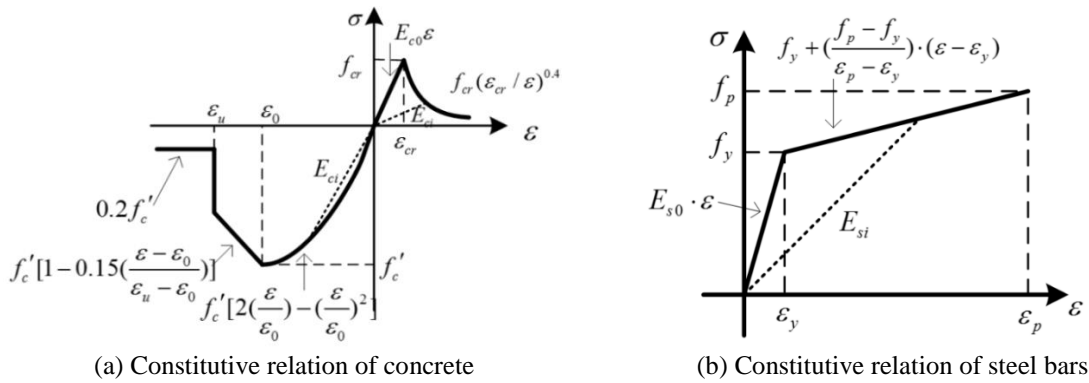


Fig. A3 Calculation of secant modulus

The constitutive relation of concrete and steel bars are shown in Fig. A3. The secant modulus of these two types of materials at a specific stress level can be obtained by evaluating the slope of the dashed lines in the figure. Therefore, to find the secant modulus, it is necessary to determine the strain associated with each segment. The longitudinal strains ε_i of the i^{th} segment can be computed from Vlasov’s elastic theory as

$$\varepsilon_i = \varphi'' \cdot \omega_i \quad (34)$$

where ω_i is the principle sectorial area coordinate of i^{th} segment, and φ'' is the curvature determined by

$$\varphi'' = -\frac{M_\omega}{I_\omega \cdot E_0} \quad (35)$$

where M_ω is the warping moment; I_ω is the principle sectorial moment of inertia; and E_0 is the initial elastic modulus of concrete. Combine Eqs. (34) and (35), the longitudinal strain of the i^{th} segment becomes

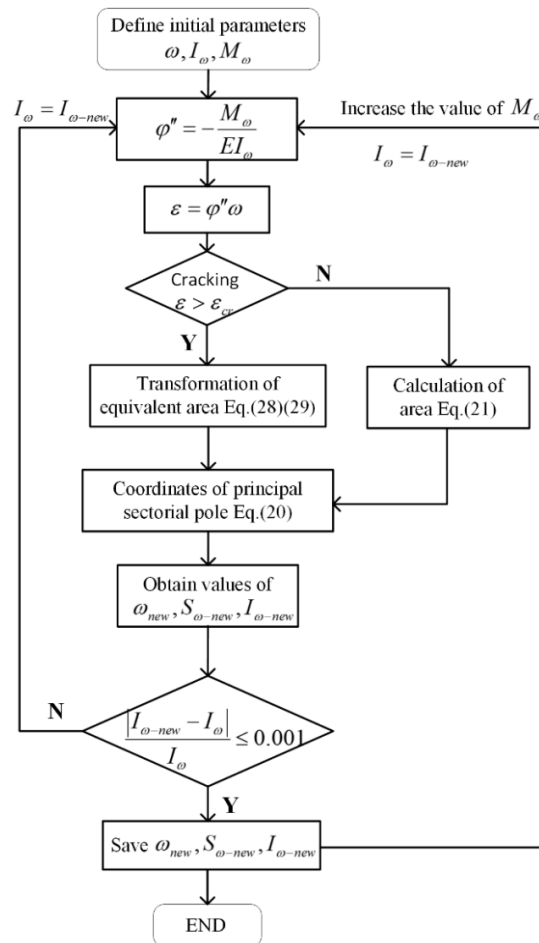


Fig. A4 Flow chart to calculate warping parameters

$$\varepsilon_i = -\frac{M_\omega}{I_\omega \cdot E_0} \omega_i \tag{36}$$

Replace Eq. (25) by Eq. (33) and repeat the procedures described in Section A.2, the warping torsional stiffness of a UTWRCM in the post-cracking stage can be derived.

The warping torsional properties of the U-shaped thin-walled RC members over the entire loading history can be calculated following the flow chart in Fig. A4. Trial and error is needed in the calculation. Figs. 10, 11 and 12 in the current paper are obtained according to the procedures outlined in this appendix.